

NLO WWZ PRODUCTION AT THE LHC

DAO Thi Nhung^{1,2*}, LE Duc Ninh^{1,2} and Marcus M. WEBER³

¹*Institut für Theoretische Physik, Karlsruher Institut für Technologie,
D-76128 Karlsruhe, Germany*

²*Institute of Physics, Vietnam Academy of Science and Technology,
10 Dao Tan, Ba Dinh, Hanoi, Vietnam*

³*Max-Planck-Institut für Physik (Werner-Heisenberg-Institut),
D-80805 München, Germany*

The tri-boson production is one of the key processes for the study of quartic gauge couplings. Next-to-leading order (NLO) corrections are mandatory to reduce theoretical uncertainties. In this study, the most up-to-date predictions including NLO QCD and NLO EW corrections to the total cross section and distributions of the W^+W^-Z production at the LHC are presented. We show that the QCD correction is about 100% and the EW correction is of a few percent at the total cross section level. The EW correction however becomes significant in the high energy regime of the gauge boson transverse momentum distributions.

1 Introduction

In the Standard Model (SM), electromagnetic and weak interactions are described by the local gauge group $SU(2)_L \otimes U(1)_Y$. According to this non-Abelian gauge structure, there exists three- and four-gauge-boson interactions. While the triple gauge couplings ($WW\gamma, WWZ$) are experimentally well understood through the analysis of two-gauge-boson production at the LEP, Tevatron and LHC (7 and 8 TeV), the understanding of quartic gauge couplings ($WW\gamma\gamma, WW\gamma Z, WWZZ, WWWW$) is less advanced. This limitation is due to the limited energy of those experiments. The direct signals of these quartic gauge couplings are obtained by either di-boson production in association with two fermions or tri-boson production which of course require high center-of-mass energy. In the next few years, operation of the upgraded LHC at 13 and 14 TeV may provide enough sensitivity for the study of the two mechanisms.

In this talk, we present a detailed study of the $pp \rightarrow W^+W^-Z$ process which is sensitive to the $WW\gamma Z$ and $WWZZ$ couplings. This process is also a background to the search of beyond SM physics. We focus on the quantum corrections to the total cross section and distributions of the process, particularly the NLO QCD and electroweak (EW) corrections. While the NLO QCD correction has been studied in Ref^{1,2}, the NLO EW correction has been recently computed by our group³. We recomputed also the NLO QCD correction and combined with the NLO EW one to provide the most up-to-date prediction for this process.

*Speaker

2 Calculation

In this section we summarize the main points of our calculation, for more details we refer to Ref³. The tree-level subprocesses are

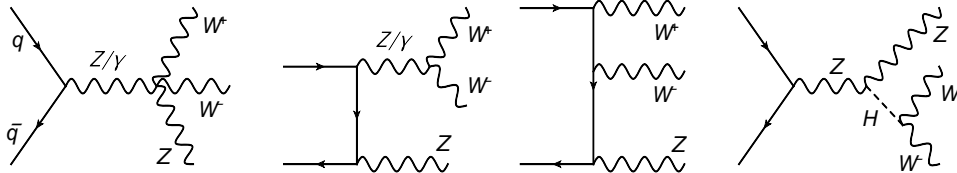


Figure 1: Representative tree-level diagrams for the $q\bar{q} \rightarrow W^+W^-Z$ subprocesses.

$$a) \bar{q} + q \rightarrow W^+ + W^- + Z, \quad b) \bar{b} + b \rightarrow W^+ + W^- + Z, \quad c) \gamma + \gamma \rightarrow W^+ + W^- + Z, \quad (1)$$

where q stands for the light quarks (u, d, c, s) if not otherwise stated. The $q\bar{q}$ contributions, whose Feynman diagrams are depicted in Fig. 1, are dominant. We include the s -channel diagrams with an intermediate Higgs boson. The Higgs contribution including interference effects is less than 1% at leading order (LO) for $M_H = 125$ GeV. The LO $b\bar{b}$ contribution is 2.4% while the LO $\gamma\gamma$ contribution is about 5% compared to the LO light quark cross section. We therefore compute NLO corrections to the light quark contribution, but not for the $b\bar{b}$ and $\gamma\gamma$ contributions.

The NLO QCD correction to $q\bar{q} \rightarrow W^+W^-Z$ consists of virtual and real corrections at the $\mathcal{O}(\alpha_s\alpha^3)$ order. The UV divergences appearing in the virtual part are isolated using dimensional regularization. The soft and collinear singularities occur in the initial state radiation of gluon (quarks) and in the virtual contribution. We have employed two methods, dimensional and mass regularizations, to separate IR singularities. The results obtained by both methods are in good agreement. To combine the virtual and real contributions we apply the dipole subtraction algorithm by Catani-Seymour⁴. The soft singularities are canceled out in the combined contribution and the left-over collinear singularities are absorbed in the quark distribution functions. To have a better understanding of the origin of large QCD corrections, we divide the QCD correction into virtual, gluon radiated and gluon-quark induced contributions. The virtual contribution consists of the QCD-loop contribution and the I-operator part arising from real radiation as defined in Ref³. The gluon radiated contribution is the remaining part of the real gluon emission process after subtracting the I-operator part.

The computation of the NLO EW correction is much more complicated in comparison with the NLO QCD correction because of the involvement of many EW particles W, Z, γ, H and fermions. The NLO EW correction contains both one-loop EW and real photonic contributions. To get the UV-finite results of the virtual part, the on-shell (OS) renormalization scheme for boson masses M_W, M_Z, M_H and external particle wave functions is employed. The G_μ scheme is applied for the electric charged e . The NLO EW contribution contains a real photon whose coupling must be defined in the Thomson limit. We therefore have to rescale the NLO EW correction with a factor of α_0/α_{G_μ} . Similar to the NLO QCD correction, we also divide the NLO EW corrections into the virtual, photon radiated and photon-quark induced contributions. Each contribution alone is free of UV and IR divergences. Mass regularization is used in combination with the dipole subtraction method⁵ to deal with IR divergences.

The matrix elements are generated with the help of `FeynArts-3.4`⁶ and `FormCalc-6.0`⁷ as well as `HELAS`^{8,9}. The maximum tensor loop integrals encountered in both QCD and EW virtual parts are the five-point tensor integrals of rank 3. The traditional Passarino-Veltman reduction¹⁰ are used for tensor reduction. The scalar and tensor one-loop integrals in one code are evaluated with the in-house library `LoopInts`. The library automatically uses quadruple precision when it detects a small Gram determinant of the N -point tensor coefficients ($N = 3, 4$). Otherwise it uses double precision.

3 Results

In this section we highlight the important numerical results for LHC 14 TeV using the MSTW2008 parton distribution function (PDF) set, for a more detailed discussion we refer to Ref³.

We start with a discussion of scale dependence. The LO total cross section including only the $q\bar{q}$ contribution depends solely on the factorization scale μ_F entering through PDFs. The NLO QCD results introduce dependence on renormalization scale μ_R through α_s . The NLO EW correction does not depend on μ_R since the OS renormalization scheme is used. For simplicity, we set $\mu_F = \mu_R = \mu$. In Fig. 2 we show the total cross sections and K-factor as functions of μ varied around the center scale μ_0 for two cases: a fixed scale with $\mu_0 = 2M_W + M_Z$ and a dynamic scale $\mu_0 = M_{WWZ}$, the invariant mass of the tri-boson system. The K-factor is defined as the ratio of the NLO QCD cross section with respect to the LO one. The strong dependence of the NLO QCD cross section on the scale is traced to the dependence of α_s on μ_R . The dynamic scale results are similar to the fixed ones for both the total cross section and the distributions we have studied. We chose the fixed scale at $\mu = 2M_W + M_Z$ for the rest of discussion.

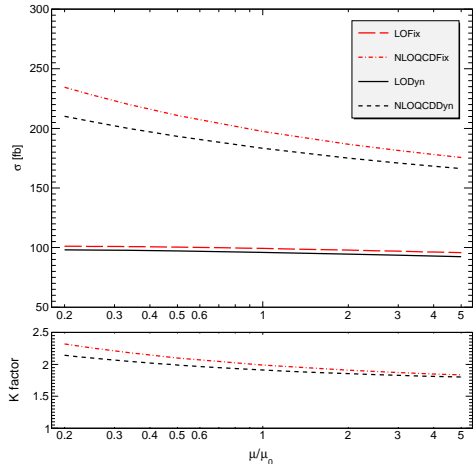


Figure 2: The total cross sections and K-factors as functions of scale.

We present the p_T distributions for the LO contribution as well as the $b\bar{b}$, $\gamma\gamma$, NLO QCD and NLO EW corrections in the left panel of Fig. 3. We take the p_T of the Z-boson as an example. The separated NLO QCD and NLO EW relative corrections compared to the LO distributions are also shown in the middle and right panels of Fig. 3, respectively. The $b\bar{b}$ and $\gamma\gamma$ contributions are about 1 to 2 orders of magnitude smaller than the $q\bar{q}$ contribution in the whole p_T range. The NLO QCD correction increases rapidly in the low p_T range and is nearly constant for $p_T > 400$ GeV. The dominant contribution comes from the gluon-induced subprocesses. The remaining contributions are less than 30%. For the NLO EW corrections, the virtual part is negative in the whole p_T range and behaves like $\alpha \log^2(M_V^2/p_T^2)$, reaching about -50% at $p_T = 1$ TeV. This is the well-known Sudakov double logarithm arising from the exchange of a virtual massive gauge boson in the loops. The photon-induced correction is about $+20\%$ at $p_{T,Z} = 1$ TeV, canceling part of the Sudakov virtual correction.

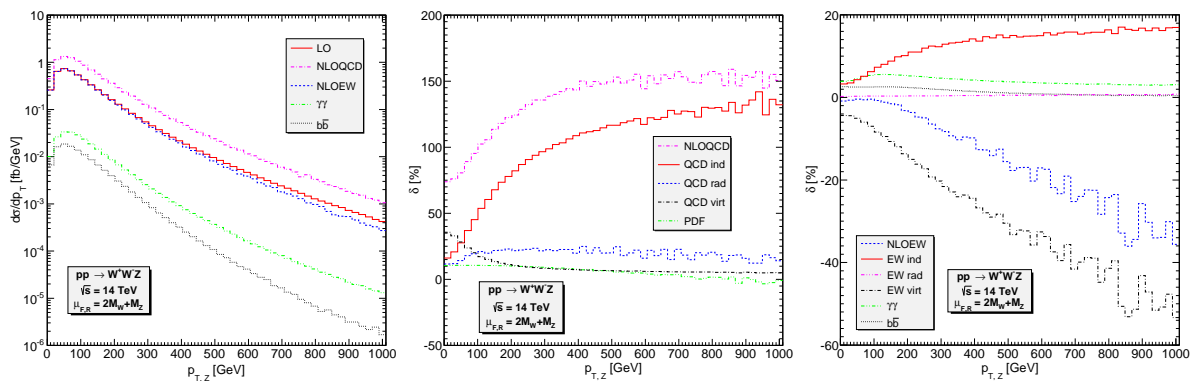


Figure 3: Z transverse momentum distribution of $pp \rightarrow W^+W^-Z$ cross section (left), of the NLO QCD corrections (middle) and of the NLO EW corrections (right).

From the above phase-space dependence study, we see that the NLO QCD correction mainly

due to the $2 \rightarrow 4$ gluon-quark induced channels is positive and very large at high p_T . The NLO EW is negative and mainly comes from the $2 \rightarrow 3$ virtual correction. One therefore thinks of imposing a jet veto to reduce this large QCD contribution. We have tried a fixed jet veto with $p_{\text{veto}} = 25$ GeV and found that it over subtracts the NLO QCD correction, leading to a large negative QCD correction at high $p_{T,Z}$, see left plot of Fig. 4. The situation is better with a dynamic jet veto with $p_{\text{veto}} = 1/2 \max(M_{T,W^+}, M_{T,W^-}, M_{T,Z})$, where $M_{T,V} = (p_{T,V}^2 + M_V^2)^{1/2}$ is the transverse mass. We found that more than half of the QCD correction is removed. However, using a jet veto increases theoretical uncertainty due to missing large higher-order corrections which is supported in the right plot of Fig. 4. The uncertainty band on the exclusive zero-jet distribution (in pink) is larger than the band on the inclusive zero-jet distribution. Note that, the uncertainty band (in black) is severely underestimated when the zero-jet and one-jet inclusive observables are wrongly assumed to be anti-correlated. The bands describe $\mu_0/2 \leq \mu_F = \mu_R \leq 2\mu_0$ with $\mu_0 = 2M_W + M_Z$ variations of the NLO QCD corrections.

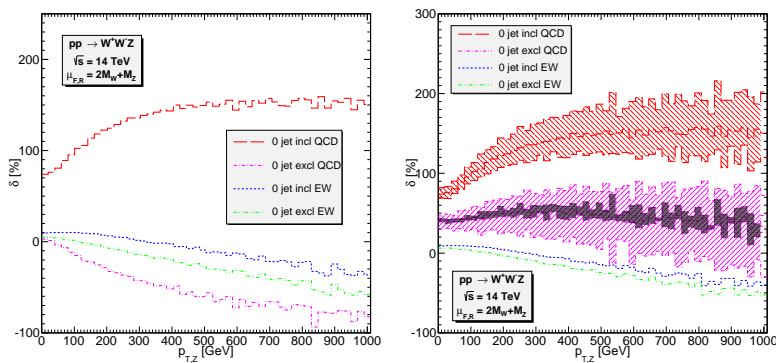


Figure 4: NLO QCD and EW corrections to the Z transverse momentum distribution for inclusive events without jet cuts and also for exclusive events with fixed jet veto (left) and dynamic jet veto with uncertainty bands (right).

4 Conclusions

In this talk, we have discussed the NLO EW and NLO QCD corrections to the W^+W^-Z production at the LHC at 14 TeV center-of-mass energy. We discussed also the use of a jet veto to reduce the large QCD correction.

Acknowledgments

D.T.N thanks the organizers for the nice atmosphere during the conference and the possibility to give talk. This work is supported by the Deutsche Forschungsgemeinschaft via the Sonderforschungsbereich/Transregio SFB/TR-9 Computational Particle Physics.

References

1. V. Hankele and D. Zeppenfeld, Phys. Lett. **B661**, 103 (2008), arXiv:0712.3544.
2. T. Binoth, G. Ossola, C. G. Papadopoulos, and R. Pittau, JHEP **06**, 082 (2008), arXiv:0804.0350.
3. D. T. Nhung, L. D. Ninh, and M. M. Weber, (2013), 1307.7403.
4. S. Catani and M. Seymour, Nucl.Phys. **B485**, 291 (1997), hep-ph/9605323.
5. S. Dittmaier, Nucl. Phys. **B565**, 69 (2000), hep-ph/9904440.
6. T. Hahn, Comput. Phys. Commun. **140**, 418 (2001), hep-ph/0012260.

7. T. Hahn and M. Perez-Victoria, *Comput. Phys. Commun.* **118**, 153 (1999), hep-ph/9807565.
8. H. Murayama, I. Watanabe, and K. Hagiwara, KEK Report No. KEK-91-11, 1992 (unpublished).
9. J. Alwall *et al.*, *JHEP* **0709**, 028 (2007).
10. G. Passarino and M. J. G. Veltman, *Nucl. Phys.* **B160**, 151 (1979).